Unfortunately, it is common practice to employ the following functions, instead of (2.72)

$$\begin{aligned} F_x &= F_x^p(F_z, \gamma, \kappa_x, \alpha, \omega_z) \\ F_y &= F_y^p(F_z, \gamma, \kappa_x, \alpha, \omega_z) \\ M_z &= M_z^p(F_z, \gamma, \kappa_x, \alpha, \omega_z) \end{aligned} \tag{2.74}$$

They are, in principle, equivalent to (2.72). However, using the longitudinal practical slip κ_x, the slip angle α and the yaw rate ω_z provides a less systematic description of the tire mechanical behavior. It looks simpler, but ultimately it is not.

2.9 Tire Testing

Tire testing aims at the full identification of the three functions (2.72) or (2.74), that is of the *relationship* between the *motion* and *position* of the rim and the *force* and *moment* exchanged with the road in the contact patch

$$\text{rim kinematics} \quad \Longleftrightarrow \quad \text{force and moment}$$

Actually, this goal had already been stated in Sect. 2.1. The difference is that now we have defined the tire slips, that is a precise set of parameters to control the rim kinematics.

Indoor tire testing facilities (Figs. 2.7 and 2.8) usually have $\omega_z = 0$ in steady-state tests, and hence lack in generality by imposing a link between γ and φ (cf. (2.60)). However, in most practical applications in road vehicles we have $|\omega_z/\omega_c| < 0.01$ and ω_z can indeed be neglected.[12]

Owing to (2.42) and (2.62), it is meaningful to perform experimental tests for the so-called *pure slip conditions*. Basically it means setting $\gamma = \varphi = 0$ and either $\sigma_y = 0$ or $\sigma_x = 0$. In the first case we have pure longitudinal slip and hence only the longitudinal force $F_x = F_x(F_z, 0, \sigma_x, 0, 0)$, which is a very special case of (2.72). In the second case we have pure lateral slip, which allows for the experimental identification of the functions $F_y = F_y(F_z, 0, 0, \sigma_y, 0)$ and $M_z = M_z(F_z, 0, 0, \sigma_y, 0)$, which are also very special cases.

Unfortunately, the practical longitudinal slip κ_x and the slip angle α usually take the place of σ_x and σ_y, respectively [2].

[12] In a step steer the steering wheel of a car may reach $\omega_z = 20°/\text{s} = 0.35$ rad/s. At a forward speed of 20 m/s, the same wheels have about $\omega_c = 80$ rad/s. The contribution of ω_z to φ is therefore like a camber angle $\gamma \approx 0.5°$.

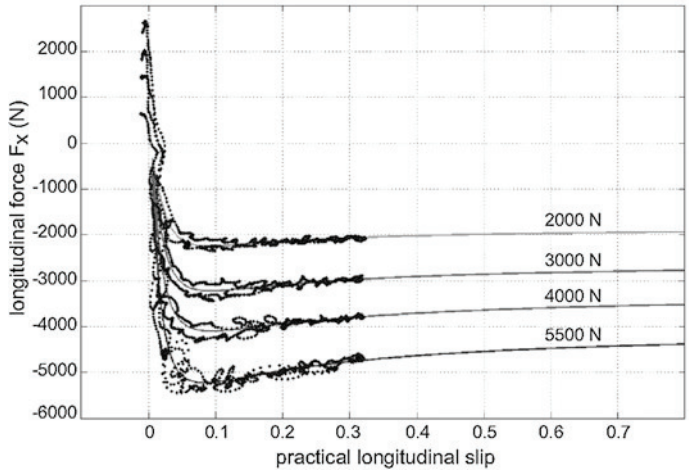

Fig. 2.15 Experimental results: longitudinal force F_x vs practical longitudinal slip κ_x for four values of the vertical load F_z

2.9.1 Pure Longitudinal Slip

Figure 2.15 shows the typical behavior of the longitudinal force F_x as a function of the practical longitudinal slip κ_x under pure braking conditions, for several values of the vertical load F_z. More precisely, it is the plot of $F_x^p(F_z, 0, \kappa_x, 0, 0)$. It is very important to note that:

- the maximum absolute value of F_x (i.e., the peak value $F_x^{\max}$) was obtained for $\kappa_x \approx 0.1$ (i.e., $\sigma_x = 0.11$);
- F_x grows *less than proportionally* with respect to the vertical load.

Both these aspects of tire behavior have great relevance in vehicle dynamics.

Also quite relevant are the values of the *longitudinal slip stiffness* C_{κ_x}, that is minus the slope of each curve at zero slip

$$C_{\kappa_x}(F_z) = -\left.\frac{\partial F_x^p}{\partial \kappa_x}\right|_{\kappa_x=0} \tag{2.75}$$

and the *global longitudinal friction coefficient* μ_p^x, that is the ratio between the peak value $F_x^{\max} = \max(|F_x^p|)$ and the corresponding vertical load

$$\mu_p^x(F_z) = \frac{F_x^{\max}}{F_z} \tag{2.76}$$

Typically, as shown in Fig. 2.16, it slightly decreases as the vertical load grows.

On the practical side, it is of some interest to observe that

- the experimental values are affected by significant errors;

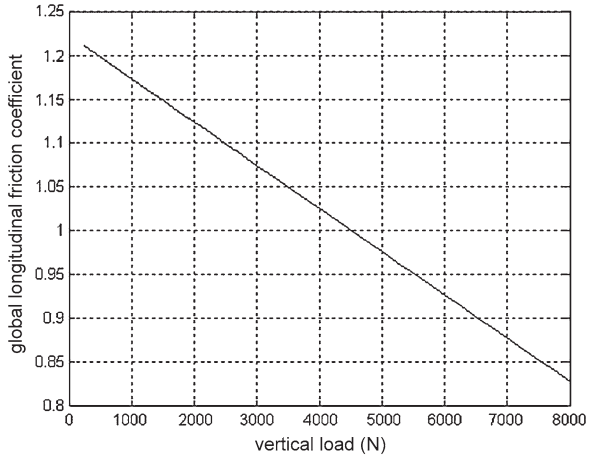

Fig. 2.16 Global longitudinal friction coefficient μ_p^x vs vertical load F_z

- the tests were carried out till $\kappa_x \approx 0.3$, to avoid wheel locking and excessive damage to the tire tread;
- the offset of F_x for $\kappa_x = 0$ is due to the rolling resistance: the wheel was (erroneously, but typically) under free rolling conditions, not pure rolling.

2.9.2 Pure Lateral Slip

Figure 2.17 shows the typical behavior of the lateral force F_y as a function of the slip angle α, for three values of F_z. More precisely, it is the plot of $F_y^p(F_z, 0, 0, \alpha, 0)$. It is very important to note that

- the maximum absolute value of F_y (i.e., the peak value $F_y^{\max}$) was obtained for $\alpha \approx \pm 8°$ (i.e., $\tan\alpha = -\sigma_y = \pm 0.14$);
- F_y grows *less than proportionally* with respect to the vertical load.

Also quite relevant are the values of the *lateral slip stiffness* C_α, also called *cornering stiffness*

$$C_\alpha(F_z) = \left.\frac{\partial F_y^p}{\partial \alpha}\right|_{\alpha=0} \tag{2.77}$$

that is the slope at the origin. As shown in Fig. 2.18, C_α grows less than proportionally with F_z, and actually it can even decrease at exceedingly high values of the vertical load.

Another important quantity is the *global lateral friction coefficient* μ_p^y, that is the ratio between the peak value $F_y^{\max} = \max(|F_y^p|)$ and the vertical load

$$\mu_p^y(F_z) = \frac{F_y^{\max}}{F_z} \tag{2.78}$$

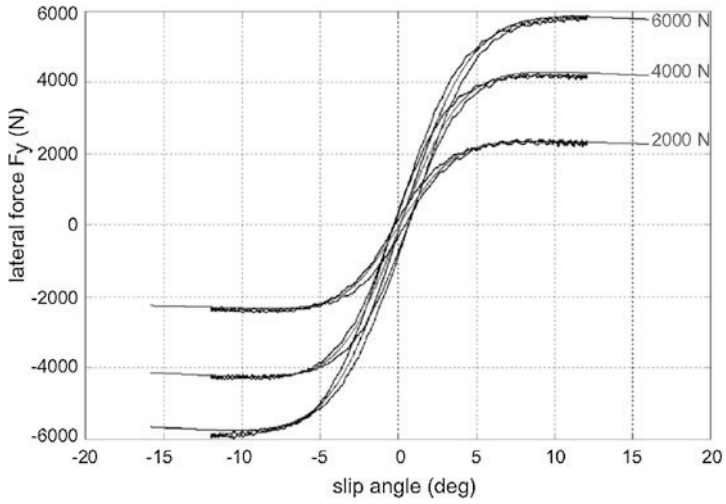

Fig. 2.17 Experimental results: lateral force F_y vs slip angle α for three values of the vertical load F_z

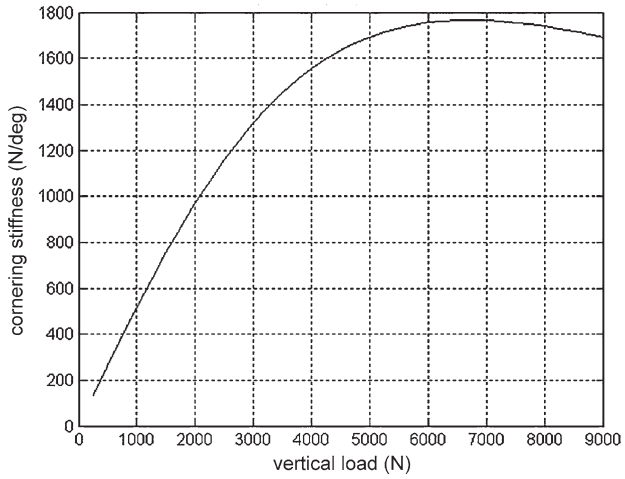

Fig. 2.18 Cornering stiffness C_α vs vertical load F_z

As shown in Fig. 2.19, it slightly decreases with F_z.

Comparing Figs. 2.16 and 2.19 we see that similar peak values for F_x and F_y are obtained for the same vertical load, that is $\mu_p^x \approx \mu_p^y$. Typically, μ_p^x is slightly greater than μ_p^y.

On the practical side it is to note that

- the experimental values are affected by small errors;
- the tests were carried out till $\alpha \approx 12°$, to avoid damaging the tire tread.

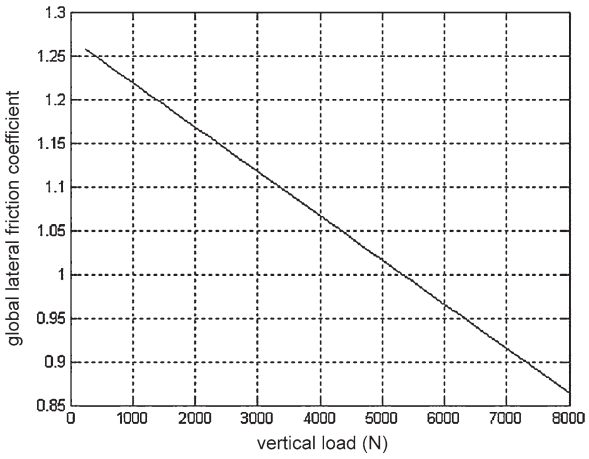

Fig. 2.19 Global lateral friction coefficient μ_p^y vs vertical load F_z

Figure 2.20 shows an example of the vertical moment M_z as a function of the slip angle α, for three values of F_z, that is the plot of $M_z^p(F_z, 0, 0, \alpha, 0)$. The tests are the same of Fig. 2.17 and similar observations apply.

The behavior of $M_z(\alpha)$ is obviously very much affected by the position of the z-axis, which should be always clearly stated. Therefore, it is hard to speak of "typical behavior" of M_z, unless there is general agreement on where to locate the origin O of the reference system. This aspect could be quite relevant in the comparison and interpretation of tests performed by different institutions, particularly for motorcycle tires at large camber angles.

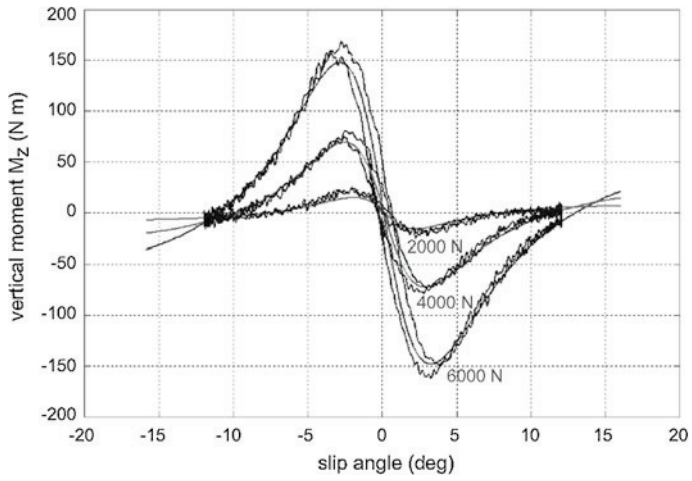

Fig. 2.20 Experimental results: vertical moment M_z vs slip angle α for three values of the vertical load F_z

2.10 Magic Formula

In vehicle dynamics it is useful to have mathematical functions that fit experimental tire response curves, like those in Figs. 2.15 and 2.17. Usually, these curves have similar shapes: they grow less than proportionally, reach a maximum and then tend to a horizontal asymptote. Among the very many functions that share all these features, there is one which is almost exclusively used in vehicle dynamics. It is called *Magic Formula* (MF).

Although, over the years, several versions of the Magic Formula have been developed, they are all based on the following function [14, 16]

$$y(x) = D \sin\Big\{C \arctan\Big[Bx - E\big(Bx - \arctan(Bx)\big)\Big]\Big\} \tag{2.79}$$

where the four coefficients are usually referred to as

$$\begin{array}{ll} B & \text{stiffness factor} \\ C & \text{shape factor} \\ D & \text{peak value} \\ E & \text{curvature factor} \end{array} \tag{2.80}$$

Of course, y can be either F_x or F_y, with x being the corresponding practical or theoretical slip component.

The Magic Formula belongs to the so-called *empirical tire models*, in the sense that they mimic some experimental curves without any relation to the physical phenomena involved in tire mechanics.

Let $B > 0$. It is quite easy to show that

- $y(0) = 0$ and $y''(0) = 0$, since $y(x) = -y(-x)$ like any anti-symmetric function;
- the slope at the origin is given by $y'(0) = BCD$;
- the value of the horizontal asymptote is $y_a = \lim_{x\to+\infty} y(x) = D \sin(C\pi/2)$, if $E < 1$;
- the function is limited: $|y(x)| \le D$;
- if $E < 1$ and $1 < C < 2$, then the function has a relative maximum $y_m = y(x_m) = D$, with

$$B(1 - E)x_m + E \arctan(Bx_m) = \tan\big(\pi/(2C)\big) \tag{2.81}$$

- $y'''(0) < 0$, if $-(1 + C^2/2) < E$.

Probably, the most relevant features of an experimental curve like in Fig. 2.17 are the peak value y_m with the corresponding abscissa x_m, the asymptotic value y_a and the slope at the origin $y'(0)$. Therefore, to determine the four coefficients a possible procedure is as follows. First set the peak value

$$D = y_m \tag{2.82}$$

then compute the shape factor C employing y_a[13]

$$C = 2 - \frac{2}{\pi} \arcsin\left(\frac{y_a}{D}\right) \tag{2.83}$$

obtain the stiffness factor B as

$$B = \frac{y'(0)}{C\,D} \tag{2.84}$$

and, finally, determine the curvature factor E from (2.81)

$$E = \frac{\tan(\pi/(2C)) - Bx_m}{\arctan(Bx_m) - Bx_m} \tag{2.85}$$

It is important that $y_a < y_m$. If they are equal (or almost equal), an unexpected plot may result. The Magic Formula usually does a good job at approximating experimental curves, although, with only four coefficients, the fitting may not be of uniform quality at all points. This aspect will be addressed in Figs. 10.16 and 10.17.

Quite often, some coefficients are made dependent on the vertical load F_z. According to Figs. 2.16 and 2.19, the global friction coefficient μ_p decreases almost linearly with F_z, and hence it is quite reasonable to assume

$$D = \mu_p F_z = (a_1 F_z + a_2) F_z \tag{2.86}$$

with $a_1 < 0$. To mimic the pattern shown in Fig. 2.18 for the slope at the origin $y'(0)$, the following formula has been suggested [16]

$$BC\,D = y'(0) = a_3 \sin\bigl(2 \arctan(F_z/a_4)\bigr) \tag{2.87}$$

Typical values may be $a_1 = -0.05\ \mathrm{kN}^{-1}$, $a_2 = 1$, $a_3 = 55$ kN/rad, $a_4 = 4$ kN.

An extensive description of the Magic Formula and all its subtleties can be found in [14].

2.11 Mechanics of Wheels with Tire

The most important aspects of tire behavior can be summarized in a few plots. They are not the whole story, and the interested reader will find in Chap. 10 many hints to better understand steady-state and also transient tire behavior. However, these plots are like a minimum common ground, i.e., something that any vehicle engineer should always have clear in mind.

Of course, they come from tire testing, either indoor or outdoor. Therefore, these plots are like the filtered (smoothed) version of the plots presented in Sect. 2.9. They were drawn employing the Magic Formula with the parameters reported below Eq. (2.87). The shape factor C was set equal to 1.65 for the plots of F_x, and equal to 1.3 for the plots of F_y.

[13] $\sin(C\pi/2) = \sin((2 - C)\pi/2)$, since $1 < C < 2$.

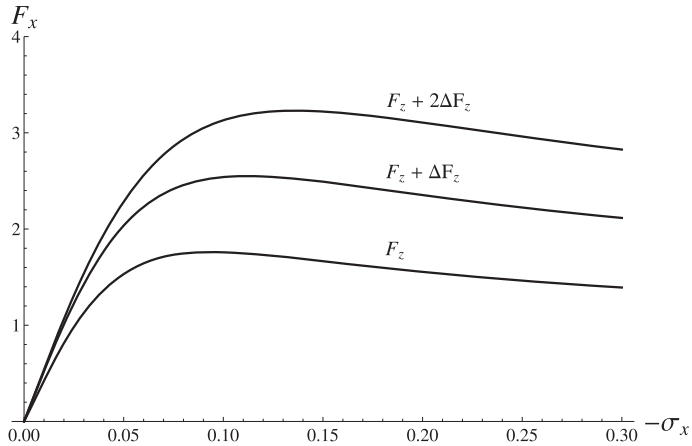

Fig. 2.21 Longitudinal force F_x due to pure longitudinal slip σ_x, for increasing vertical loads F_z. More precisely $F_x = F_x(F_z, 0, \sigma_x, 0, 0)$

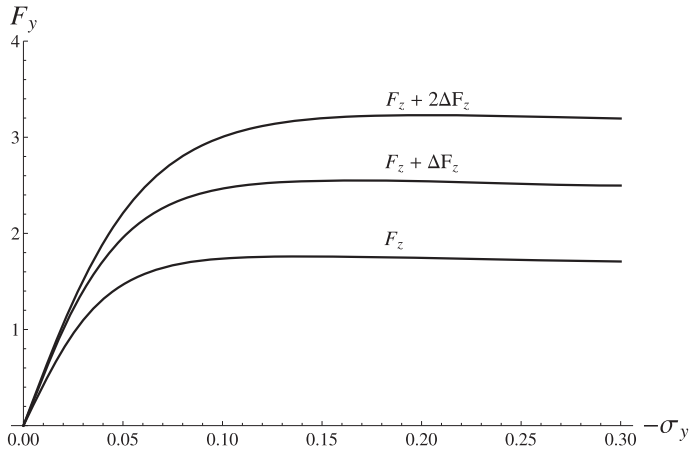

Fig. 2.22 Lateral force F_y due to pure lateral slip σ_y, for increasing vertical loads F_z. More precisely $F_y = F_y(F_z, 0, 0, \sigma_y, 0)$

Most tires under pure longitudinal slip behave like in Fig. 2.21. In particular, the effect of increasing the vertical load F_z is shown. As already mentioned at p. 34, the growth of F_x is less than proportional, particularly for low values of σ_x.

Similarly, most tires under pure lateral slip behave like in Fig. 2.22. In particular, the effect of increasing the vertical load F_z is shown. Again, as already mentioned at p. 35, the growth of F_y is less than proportional, particularly for low values of σ_y. It is precisely this nonlinearity that is, let us say, activated by anti-roll bars to modify the handling set-up of a car.

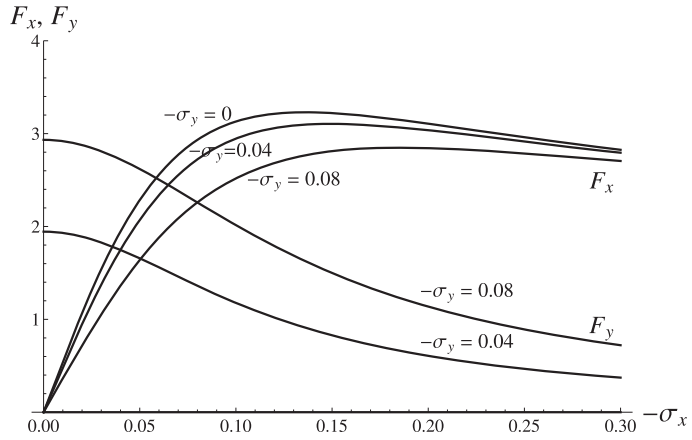

Fig. 2.23 Longitudinal force F_x and lateral force F_y due to combined longitudinal slip σ_x and lateral slip σ_y, for constant vertical load F_z. More precisely $F_y = F_y(F_z, 0, \sigma_x, \sigma_y, 0)$ and $F_y = F_y(F_z, 0, \sigma_x, \sigma_y, 0)$

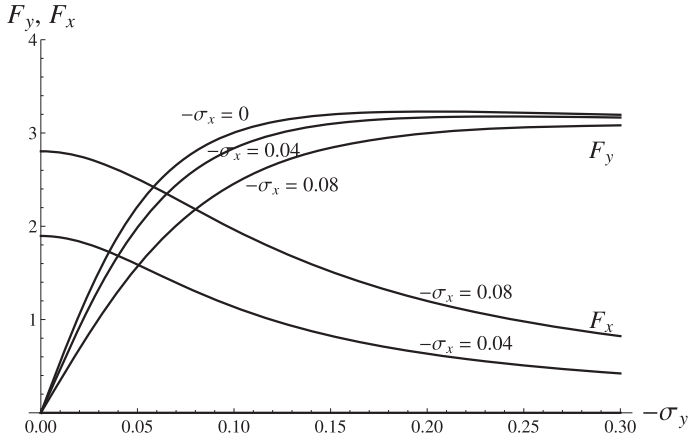

Fig. 2.24 Longitudinal force F_x and lateral force F_y due to combined longitudinal slip σ_x and lateral slip σ_y, for constant vertical load F_z. More precisely $F_y = F_y(F_z, 0, \sigma_x, \sigma_y, 0)$ and $F_y = F_y(F_z, 0, \sigma_x, \sigma_y, 0)$

The simultaneous application of σ_x and σ_y affects the grip forces F_x and F_y the way shown in Figs. 2.23 and 2.24. Basically, the total force $\mathbf{F}_t$, with components F_x and F_y, is directed like the slip vector $\boldsymbol{\sigma}$, with opposite sign, and has a magnitude almost dependent on $|\boldsymbol{\sigma}|$. These aspects will be thoroughly addressed in Chap. 10, were the tire brush model will be developed.

Also very relevant is the effect of the camber angle γ, alone or in combination with σ_y, on the lateral force F_y, as shown in Fig. 2.25 and, for better clarity, also in Fig. 2.26. We see that the camber effects are much stronger at low values of σ_y.

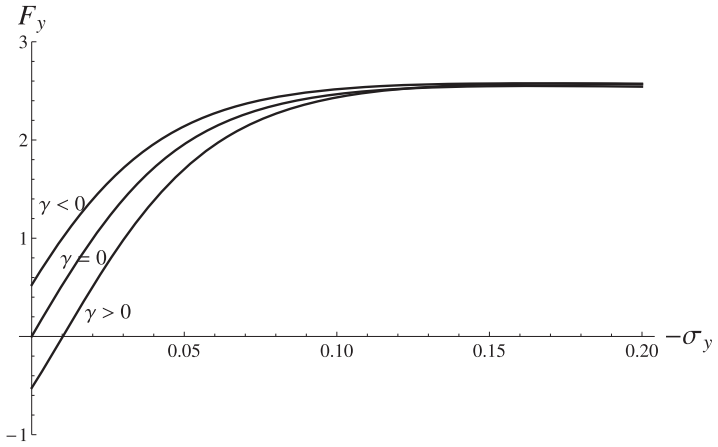

Fig. 2.25 Lateral force F_y due to lateral slip σ_y, for different values of the camber angle γ and constant vertical load F_z. More precisely $F_y = F_y(F_z, \gamma, 0, \sigma_y, 0)$

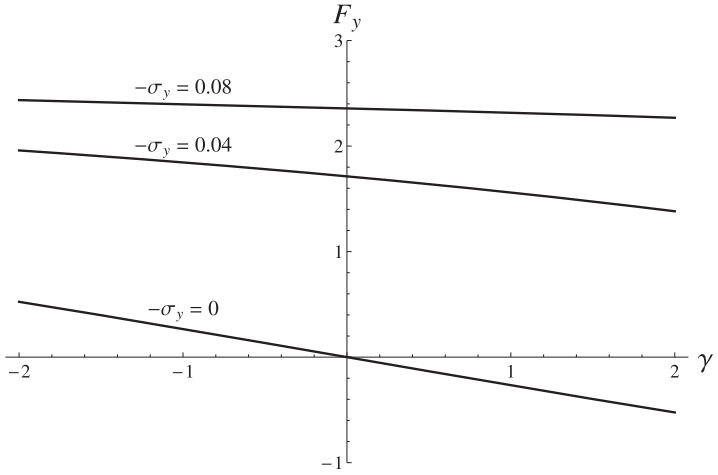

Fig. 2.26 Lateral force F_y due to camber angle γ, for different values of the lateral slip σ_y and constant vertical load F_z. More precisely $F_y = F_y(F_z, \gamma, 0, \sigma_y, 0)$

However, a right amount of camber can increase the maximum lateral force, thus improving the car handling performance.

Finally, the effect of the increasing the grip coefficient μ is investigated. We see in Figs. 2.27 and 2.28 that, as expected, we get higher maximum tangential forces. However, it should also be noted that changing the grip does not affect the slope of the curves near the origin.

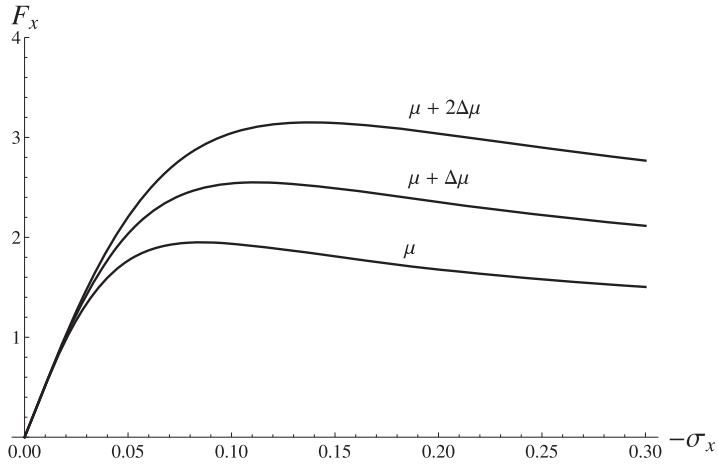

Fig. 2.27 Longitudinal force F_x due to pure longitudinal slip σ_x, for constant vertical load F_z and increasing grip

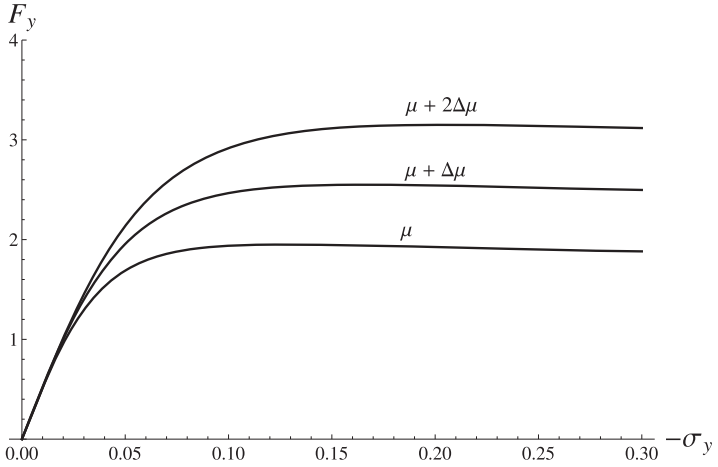

Fig. 2.28 Lateral force F_y due to pure lateral slip σ_y, for constant vertical load F_z and increasing grip

2.12 Summary

In this chapter we have first pursued the goal of clearly describing the relevant kinematics of a wheel with tire, mainly under steady-state conditions. This had led to the definitions of slips as a measure of the extent to which the wheel with tire departs from pure rolling conditions. The slip angle has been also defined and discussed. It has been shown that a wheel with tire resembles indeed a rigid wheel because slip angles are quite small. Tire experimental tests shows the relationships between the

kinematics and the forces/couples the tire exchanges with the road. The Magic Formula provides a convenient way to represent these functions. Finally, the mechanics of the wheel with tire has been summarized with the aid of a number of plots.

2.13 List of Some Relevant Concepts

p. 8 a wheel with tire is barely a wheel;
p. 11 there are two distinct contributions to the spin velocity of the rim;
p. 11 in a wheel, longitudinal velocities are expected to be much higher than lateral ones;
p. 15 the name "self-aligning torque" is meaningless and even misleading;
p. 21 rim kinematics depends on six variables, but often (not always) only five may be relevant for the tire;
p. 22 a reasonable definition of pure rolling for a wheel with tire is that the grip actions $\mathbf{t}$ have no global effect;
p. 20 pure rolling and free rolling are different concepts;
p. 27 tire slips measure the distance from pure rolling;
p. 30 tire slips do not provide any direct information on the amount of sliding at any point of the contact patch;
p. 32 tire forces and moments depend on both the camber angle γ and the spin slip φ.

References

1. Bastow D, Howard G, Whitehead JP (2004) Car suspension and handling, 4th edn. SAE International, Warrendale
2. Bergman W (1977) Critical review of the state-of-the-art in the tire and force measurements. SAE Preprint (770331)
3. Clark SK (ed) (2008) The pneumatic tire. NHTSA–DOT HS 810 561
4. Dixon JC (1991) Tyres, suspension and handling. Cambridge University Press, Cambridge
5. Font Mezquita J, Dols Ruiz JF (2006) La Dinámica del Automóvil. Editorial de la UPV, Valencia
6. Gillespie TD (1992) Fundamentals of vehicle dynamics. SAE International, Warrendale
7. Meirovitch L (1970) Methods of analytical dynamics. McGraw-Hill, New York
8. Michelin (2001) The tyre encyclopaedia. Part 1: grip. Société de Technologie Michelin, Clermont–Ferrand [CD-ROM]
9. Michelin (2002) The tyre encyclopaedia. Part 2: comfort. Société de Technologie Michelin, Clermont–Ferrand [CD-ROM]
10. Michelin (2003) The tyre encyclopaedia. Part 3: rolling resistance. Société de Technologie Michelin, Clermont–Ferrand [CD-ROM]
11. Milliken WF, Milliken DL (1995) Race car vehicle dynamics. SAE International, Warrendale
12. Murray RM, Li Z, Sastry SS (1994) A mathematical introduction to robot manipulation. CRC Press, Boca Raton
13. Pacejka HB (1996) The tyre as a vehicle component. In: 26th FISITA congress '96: engineering challenge human friendly vehicles, Prague, June 17–21, pp 1–19